

**HYDROGEN GAS SENSORS BASED ON  
NANOCRYSTALLINE SnO<sub>2</sub> THIN FILMS  
GROWN ON DIFFERENT SUBSTRATES USING  
SOL-GEL SPIN COATING METHOD**

by

**IMAD HUSSEIN KADHIM**

**Thesis submitted in fulfillment of the requirements  
for the degree of  
Doctor of Philosophy**

**May 2017**

## **ACKNOWLEDGEMENT**

First and foremost, I would like to thank Allah for granting me health and patience to finish this research. I would also like to express my sincere gratitude to my main supervisor, Prof. Dr. Haslan Abu Hassan, for his valuable guidance and support throughout these study years. He also taught me to overcome all the problems and solved them, and I am grateful for his confidence, kindness and patience with my research. I consider myself very lucky and most honored to be one of his students. Thank you professor for having your door open every time I needed help.

My appreciation also goes to the staffs of the Nano-Optoelectronics Research and Technology Laboratory (NOR Lab) and Solid-state laboratory for their technical assistance during my laboratory work.

Many thanks to my friend Ammar, and to all my friends and colleagues who supported and helped me at the School of Physics, Universiti Sains Malaysia.

The prayers of my father, the support of my brothers and sister, and the remembrance of my mother and sisters were a powerful source in completing this research. Last and most important, I extend special thanks to my wife (Alaa) and my children (Marem, Haithem, and Mohammed) for the patience and accompanying me during this important time in our lives.

## TABLE OF CONTENTS

ACKNOWLEDGEMENT.....	ii
TABLE OF CONTENTS.....	iii
LIST OF TABLES.....	vii
LIST OF FIGURES.....	ix
LIST OF SYMBOLS.....	xvi
LIST OF ABBREVIATIONS.....	xviii
ABSTRAK.....	xix
ABSTRACT.....	xxii
 <b>CHAPTER 1: INTRODUCTION</b>	
1.1 Overview.....	1
1.2 Motivations and problem statements.....	2
1.3 Scope of study.....	4
1.4 Objectives of the research.....	5
1.5 Originality of the research.....	5
1.6 Outline of the research.....	6
 <b>CHAPTER 2: LITERATURE REVIEW AND THEORETICAL BACKGROUND</b>	
2.1 Introduction.....	8
2.2 Nanomaterials.....	8

2.3	Literature review for the growth of SnO <sub>2</sub> nanostructures and gas sensors based on SnO <sub>2</sub> nanostructures.....	9
2.3.1	Growth of SnO <sub>2</sub> nanostructures .....	9
2.3.2	Sol-gel spin coating method .....	9
2.3.3	Growth mechanism of SnO <sub>2</sub> thin film using sol-gel spin coating method.....	16
2.3.4	Glycerin as biding agent.....	16
2.3.5	SnO <sub>2</sub> morphology changes with annealing temperature.....	17
2.3.6	Gas sensor based on SnO <sub>2</sub> nanostructures.....	16
2.4	Theoretical background .....	24
2.4.1	Structural properties of SnO <sub>2</sub> .....	24
2.4.2	Surface properties of SnO <sub>2</sub> nanostructutres .....	26
2.4.3	Metal-semiconductor contact.....	27
2.4.3(a)	Schottky contact.....	28
2.4.3(b)	Ohmic contact .....	31
2.4.4	Gas sensing properties.....	32
2.4.5	Sensing mechanism of the SnO <sub>2</sub> nanostructures.....	33
2.5	Summary.....	35

### **CHAPTER 3: METHODOLOGY AND INSTRUMENTS**

3.1	Introduction.....	36
3.2	The parameters proposed in this work.....	36
3.3	Systematic approach of the fabrication of gas sensor based on NC SnO <sub>2</sub> thin films .....	36
3.4	Cleaning substrates.....	40
3.4.1	Oxidation of SiO <sub>2</sub> .....	41
3.5	Preparation of SnO <sub>2</sub> sol solutions.....	41

3.6	Aging heat times.....	42
3.7	Spin coating process .....	42
3.8	Annealing process .....	43
3.9	Principles of the characterization instruments .....	43
3.9.1	X-ray diffraction system.....	44
3.9.2	Field emission scanning electron microscope and energy dispersive X-ray spectroscopy.....	47
3.9.3	Raman spectroscopy.....	48
3.10	Fabrication of MSM gas sensor based on NC SnO <sub>2</sub> thin films.....	50
3.10.1	Shadow grid mask.....	51
3.10.2	RF-sputtering system.....	51
3.11	Gas sensing test system .....	52
3.12	Summary.....	55

**CHAPTER 4: RESULTS AND DISCUSSION FOR GROWTH AND CHARACTERIZATION OF NANOCRYSTALLINE SnO<sub>2</sub> THIN FILMS GROWN ON DIFFERENT SUBSTRATES**

4.1	Introduction.....	56
4.2	Growth and characterizations of nanocrystalline SnO <sub>2</sub> thin films deposited on bare Si (100), SiO <sub>2</sub> /Si and Al <sub>2</sub> O <sub>3</sub> substrates.....	56
4.2.1	Growth of nanocrystalline SnO <sub>2</sub> thin films .....	56
4.2.2	Characterizations of nanocrystalline SnO <sub>2</sub> thin films .....	57
4.2.2(a)	XRD analysis .....	57
4.2.2(b)	FESEM observation.....	68
4.2.2(c)	EDX observation .....	77
4.2.2(d)	Raman spectroscopy.....	84
4.2.3	Effect of aging heat times on nanocrystalline SnO <sub>2</sub> .....	91
4.2.3(a)	XRD analysis .....	91

4.2.3(b) FESEM observation.....	106
4.2.3(c) EDX observation .....	106
4.2.3(d) Effects of aging heat times on thin films thickness.....	111
4.2.3(e) Raman spectroscopy .....	114
4.3 Summary.....	120

**CHAPTER 5: RESULTS AND DISCUSSION FOR H<sub>2</sub> GAS SENSORS  
BASED ON NANOCRYSTALLINE SnO<sub>2</sub> THIN FILMS  
GROWN ON DIFFERENT SUBSTRATES**

5.1 Introduction.....	121
5.2 Fabricated devices .....	121
5.3 Metal-semiconductor-metal H <sub>2</sub> gas sensors.....	121
5.3.1 Electrical characterization .....	122
5.4 Hydrogen gas sensor based on nanocrystalline SnO <sub>2</sub> thin films grown on bare Si (100) substrates.....	125
5.5 Hydrogen gas sensor based on nanocrystalline SnO <sub>2</sub> thin films grown on SiO <sub>2</sub> /Si substrates .....	131
5.6 Hydrogen gas sensor based on nanocrystalline SnO <sub>2</sub> thin films grown on Al <sub>2</sub> O <sub>3</sub> substrates.....	135
5.7 Summary.....	141

**CHAPTER 6: CONCLUSIONS AND FUTURE WORKS**

6.1 Conclusions.....	142
6.2 Future works.....	145

<b>REFERENCES.....</b>	<b>147</b>
------------------------	------------

**APPENDIX**

**LIST OF PUBLICATIONS**

## LIST OF TABLES

	Page
Table 2.1: Summary of the NC SnO <sub>2</sub> thin films prepared using sol-gel spin coating method. ....	15
Table 2.2: Summary of the sensitivity, the response and recovery times for the SnO <sub>2</sub> nanostructure based gas sensor. ....	23
Table 2.3: Chemical and physical properties of SnO <sub>2</sub> . ....	25
Table 4.1: Summary of XRD analysis for the NC SnO <sub>2</sub> thin films for different glycerin volume ratios and annealing temperatures grown on bare Si (100) substrates. ....	63
Table 4.2: Summary of XRD analysis for the NC SnO <sub>2</sub> thin films for different glycerin volume ratios and annealing temperatures grown on SiO <sub>2</sub> /Si substrates. ....	65
Table 4.3: Summary of XRD analysis for the NC SnO <sub>2</sub> thin films for different glycerin volume ratios and annealing temperatures grown on Al <sub>2</sub> O <sub>3</sub> substrates. ....	67
Table 4.4 : Summary of XRD analysis for the NC SnO <sub>2</sub> thin films for different aging heat times and annealing temperatures grown on bare Si (100) substrates. ....	95
Table 4.5: Summary of XRD analysis for the NC SnO <sub>2</sub> thin films for different aging heat times and annealing temperatures grown on SiO <sub>2</sub> /Si substrates. ....	97
Table 4.6: Summary of XRD analysis for the NC SnO <sub>2</sub> thin films for different aging heat times and annealing temperatures grown on Al <sub>2</sub> O <sub>3</sub> substrates. ....	99
Table 5.1: Schottky barrier height ( $\phi_B$ ), ideality factor ( $n$ ) and rectifying ratio ( $I_F/I_R$ ) of the fabricated devices. ....	123
Table 5.2: The comparison between previous studies and present work of the sensitivity, the response and recovery times for NC SnO <sub>2</sub> thin film sensor (Device 1) grown on bare Si (100) substrates at different operating temperatures. ....	131
Table 5.3: The comparison between previous studies and the present work of the sensitivity, the response and recovery times for the NC SnO <sub>2</sub> thin film sensor grown on SiO <sub>2</sub> /Si substrates at different operating temperatures. ....	135

Table 5.4: The comparison between sensing capability of the previous studies and present work related to the sensitivity, the response and recovery times for the NC SnO<sub>2</sub> thin film sensor grown on Al<sub>2</sub>O<sub>3</sub> substrates at different operating temperatures. .... 139



## LIST OF FIGURES

	<b>Page</b>
Figure 2.1: Spin coating process (a) spin coating system, (b) the four steps involved [50].	11
Figure 2.2: Hydrogen bonding between glycerin and the compounds of SnCl <sub>2</sub> and Sn(OH) <sub>2</sub> .	17
Figure 2.3: Crystalline structure of SnO <sub>2</sub> [93].	25
Figure 2.4: The general schematic band diagram of bulk SnO <sub>2</sub> [99].	27
Figure 2.5: Energy band diagram of perfect metal and n-type semiconductor Schottky contact under thermal equilibrium (a) before contact and (b) after contact [102].	28
Figure 2.6: Energy band diagram of perfect metal and n-type semiconductor ohmic contact under thermal equilibrium (a) before contact and (b) after contact [103].	32
Figure 2.7: Crystal grains contact/boundary of metal oxide semiconductor (a) in air and (b) in reduction H <sub>2</sub> gas [113].	34
Figure 2.8: Sensing mechanisms of SnO <sub>2</sub> based sensor: (a) in air and (b) in the reduction H <sub>2</sub> gas [114].	35
Figure 3.1: Flowchart of the fabrication of H <sub>2</sub> gas sensor based on NC SnO <sub>2</sub> thin films using sol-gel spin coating method.	39
Figure 3.2: The general diagram for the preparation of SnO <sub>2</sub> sol solutions using the magnetic stirrer.	42
Figure 3.3: The schematic diagram of a thermal annealing tube furnace.	43
Figure 3.4: The schematic diagram of an X-ray diffraction experiment [118].	44
Figure 3.5: Diffraction of an X-ray beam by crystal planes [118].	45
Figure 3.6: Schematic diagram of FESEM [127].	48
Figure 3.7: Schematic diagram of the two types of Raman scattering processes [129].	49
Figure 3.8: Schematic diagram of the Raman spectroscopy system [132].	50
Figure 3.9: The dimensions of the shadow grid mask.	51

Figure 3.10: Schematic diagram of an RF magnetron sputtering system [134].	52
Figure 3.11: Schematic diagram of H <sub>2</sub> gas sensor testing system.	54
Figure 3.12: The response and recovery times of MSM based a gas sensor [138].	55
Figure 4.1: XRD patterns of glycerin-free SnO <sub>2</sub> thin films prepared from sol solution aging for 8 h at 70 °C grown on different substrates.	58
Figure 4.2: XRD patterns of SnO <sub>2</sub> thin films prepared from sol solution with glycerin volume ratio (1:12) and aging for 8 h at 70 °C grown on different substrates.	60
Figure 4.3: XRD patterns of SnO <sub>2</sub> thin films prepared from sol solution with glycerin volume ratio (1:8) and aging for 8 h at 70 °C grown on different substrates.	62
Figure 4.4: FESEM images of glycerin-free SnO <sub>2</sub> thin films prepared from sol solution aging for 8 h at 70 °C grown on bare Si (100) substrates. The insert images show the FESEM images taken at higher magnification (100,000x)	69
Figure 4.5: FESEM images of SnO <sub>2</sub> thin films prepared from sol solution aging for 8 h at 70 °C with glycerin volume ratio (1:12) grown on bare Si (100) substrates. The insert images show the FESEM images taken at higher magnification (100,000x)	70
Figure 4.6: FESEM images of SnO <sub>2</sub> thin films prepared from sol solution aging for 8 h at 70 °C with glycerin volume ratio (1:8) grown on bare Si (100) substrates. The insert images show the FESEM images taken at higher magnification (100,000x)	71
Figure 4.7: FESEM images of glycerin-free of SnO <sub>2</sub> thin films prepared from sol solution aging for 8 h at 70 °C grown on SiO <sub>2</sub> /Si substrates. The insert images show the FESEM images taken at higher magnification (100,000x)	72
Figure 4.8: FESEM images of SnO <sub>2</sub> thin films prepared from sol solution aging for 8 h at 70 °C with glycerin volume ratio (1:12) grown on SiO <sub>2</sub> /Si substrates. The insert images show the FESEM images taken at higher magnification (100,000x)	73
Figure 4.9: FESEM images of SnO <sub>2</sub> thin films prepared from sol solution aging for 8 h at 70 °C with glycerin volume ratio (1:8) grown on SiO <sub>2</sub> /Si substrates. The insert images show the FESEM images taken at higher magnification (100,000x)	74
Figure 4.10: FESEM images of glycerin-free of SnO <sub>2</sub> thin films prepared from sol solution aging for 8 h at 70 °C grown on Al <sub>2</sub> O <sub>3</sub> substrates. The	

insert images show the FESEM images taken at higher magnification (100,000x) .....	75
Figure 4.11: FESEM images of SnO <sub>2</sub> thin films prepared from sol solution aging for 8 h at 70 °C with glycerin volume ratio (1:12) grown on Al <sub>2</sub> O <sub>3</sub> substrates. The insert images show the FESEM images taken at higher magnification (100,000x).....	76
Figure 4.12: FESEM images of SnO <sub>2</sub> thin films prepared from sol solution aging for 8 h at 70 °C with glycerin volume ratio (1:8) grown on Al <sub>2</sub> O <sub>3</sub> substrates. The insert images show the FESEM images taken at higher magnification (100,000x).....	76
Figure 4.13: EDX spectra of glycerin-free SnO <sub>2</sub> thin films prepared from sol solution aging for 8 h at 70 °C grown on bare Si (100) substrates. ....	77
Figure 4.14: EDX spectra of SnO <sub>2</sub> thin films prepared from sol solution aging for 8 h at 70 °C with glycerin volume ratio (1:12) grown on bare Si (100) substrates. ....	78
Figure 4.15: EDX spectra of SnO <sub>2</sub> thin films prepared form sol solution aging for 8 h at 70 °C with glycerin volume ratio (1:8) grown on bare Si (100) substrates. ....	79
Figure 4.16: EDX spectra of glycerin-free SnO <sub>2</sub> thin films prepared from sol solution aging for 8 h at 70 °C grown on SiO <sub>2</sub> /Si substrates.....	80
Figure 4.17: EDX spectra of SnO <sub>2</sub> thin films prepared from sol solution aging for 8 h at 70 °C with glycerin volume ratio (1:12) grown on SiO <sub>2</sub> /Si substrates. ....	80
Figure 4.18: EDX spectra of SnO <sub>2</sub> thin films prepared from sol solution aging for 8 h at 70 °C with glycerin volume ratio (1:8) grown on SiO <sub>2</sub> /Si substrates.....	81
Figure 4.19: EDX spectra of glycerin-free SnO <sub>2</sub> thin films prepared from sol solution aging for 8 h at 70 °C grown on Al <sub>2</sub> O <sub>3</sub> substrates. ....	82
Figure 4.20: EDX spectra of SnO <sub>2</sub> thin films prepared from sol solution aging for 8 h at 70 °C with glycerin volume ratio (1:12) grown on Al <sub>2</sub> O <sub>3</sub> substrates.....	83
Figure 4.21: EDX spectra of SnO <sub>2</sub> thin films prepared from sol solution aging for 8 h at 70 °C with glycerin volume ratio (1:8) grown on Al <sub>2</sub> O <sub>3</sub> substrates. ....	83
Figure 4.22: EDX results in terms of elements and the weight versus annealing temperatures of NC SnO <sub>2</sub> thin films prepared from sol solutions (a) glycerin-free, (b) with (1:12) glycerin volume ratio and (c) with (1:8) glycerin volume ratio.....	84

Figure 4.23: Raman spectra of glycerin-free SnO <sub>2</sub> thin films prepared from sol solution aging for 8 h at 70 °C grown on different substrates. ....	86
Figure 4.24: Raman spectra of SnO <sub>2</sub> thin films prepared from sol solution aging for 8 h at 70 °C with glycerin volume ratio (1:12) grown on different substrates. ....	87
Figure 4.25: Raman spectra of SnO <sub>2</sub> thin films prepared from sol solution aging for 8 h at 70 °C with glycerin volume ratio (1:8) grown on different substrates.....	89
Figure 4.26: The values of A <sub>1g</sub> mode versus annealing temperatures of NC SnO <sub>2</sub> thin films prepared from sol solutions (a) glycerin-free, (b) with (1:12) glycerin volume ratio and (c) with (1:8) glycerin volume ratio.....	90
Figure 4.27: XRD patterns of SnO <sub>2</sub> thin films prepared from sol solution aging for (a) 24 h at RT and aging at 70 °C for; (b) 6 h and (c) 10 h grown on different substrates.....	93
Figure 4.28: FESEM images of SnO <sub>2</sub> thin films prepared from sol solution aging for 24 h at RT grown on bare Si (100) substrates. The insert images show the FESEM images taken at higher magnification (100,000x).....	101
Figure 4.29: FESEM images of SnO <sub>2</sub> thin films prepared from sol solution aging for 6 h at 70 °C grown on bare Si (100) substrates. The insert images show the FESEM images taken at higher magnification (100,000x).....	101
Figure 4.30: FESEM images of SnO <sub>2</sub> thin films prepared from sol solution aging for 10 h at 70 °C grown on bare Si (100) substrates. The insert images show the FESEM images taken at higher magnification (100,000x).....	102
Figure 4.31: FESEM images of SnO <sub>2</sub> thin films prepared from sol solution aging for 24 h at RT grown on SiO <sub>2</sub> /Si substrates. The insert images show the FESEM images taken at higher magnification (100,000x).....	103
Figure 4.32: FESEM images of SnO <sub>2</sub> thin films prepared from sol solution aging for 6 h at 70 °C grown on SiO <sub>2</sub> /Si substrates. The insert images show the FESEM images taken at higher magnification (100,000x).....	103
Figure 4.33: FESEM images of SnO <sub>2</sub> thin films prepared from sol solution aging for 10 h at 70 °C grown on SiO <sub>2</sub> /Si substrates. The insert images show the FESEM images taken at higher magnification (100,000x).....	104
Figure 4.34: FESEM images of SnO <sub>2</sub> thin films prepared from sol solution aging for 24 h at RT grown on Al <sub>2</sub> O <sub>3</sub> substrates. The insert images show the FESEM images taken at higher magnification (100,000x).....	105

Figure 4.35: FESEM images of SnO <sub>2</sub> thin films prepared from sol solution aging for 6 h at 70 °C grown on Al <sub>2</sub> O <sub>3</sub> substrates. The insert images show the FESEM images taken at higher magnification (100,000x).....	105
Figure 4.36: FESEM images of SnO <sub>2</sub> thin films prepared from sol solution aging for 10 h at 70 °C grown on Al <sub>2</sub> O <sub>3</sub> substrates. The insert images show the FESEM images taken at higher magnification (100,000x).....	106
Figure 4.37: EDX spectra of SnO <sub>2</sub> thin films prepared from sol solution aging for 24 h at RT grown on bare Si (100) substrates. ....	107
Figure 4.38: EDX spectra of SnO <sub>2</sub> thin films prepared from sol solution aging for 6 h at 70 °C grown on bare Si (100) substrates. ....	107
Figure 4.39: EDX spectra of SnO <sub>2</sub> thin films prepared from sol solution aging for 10 h at 70 °C grown on bare Si (100) substrates. ....	108
Figure 4.40: EDX spectra of SnO <sub>2</sub> thin films prepared and aging for 24 h at RT grown on SiO <sub>2</sub> /Si substrates.....	108
Figure 4.41: EDX spectra of SnO <sub>2</sub> thin films prepared from sol solution aging for 6 h at 70 °C grown on SiO <sub>2</sub> /Si substrates.....	109
Figure 4.42: EDX spectra of SnO <sub>2</sub> thin films prepared from sol solution aging for 10 h at 70 °C grown on SiO <sub>2</sub> /Si substrates.....	109
Figure 4.43: EDX spectra of SnO <sub>2</sub> thin films prepared from sol solution aging at RT grown on Al <sub>2</sub> O <sub>3</sub> substrates.....	110
Figure 4.44: EDX spectra of SnO <sub>2</sub> thin films prepared from sol solution aging for 6 h at 70 °C grown on Al <sub>2</sub> O <sub>3</sub> substrates. ....	110
Figure 4.45: EDX spectra of SnO <sub>2</sub> thin films prepared from sol solution aging for 10 h at 70 °C grown on Al <sub>2</sub> O <sub>3</sub> substrates. ....	111
Figure 4.46: FESEM cross-section micrographs of as-deposited SnO <sub>2</sub> thin films prepared from sol solutions aging at (a) for 24 h at RT and for (b) 6 h, (c) 8 h and (d) 10 h at 70 °C grown on bare Si (100) substrates.....	112
Figure 4.47: FESEM cross-section micrographs of as-deposited SnO <sub>2</sub> thin films prepared from sol solutions aging at (a) for 24 h at RT and for (b) 6 h, (c) 8 h and (d) 10 h at 70 °C grown on SiO <sub>2</sub> /Si substrates. ....	113
Figure 4.48: FESEM cross-section micrographs of as-deposited SnO <sub>2</sub> thin films prepared from sol solutions aging at (a) for 24 h at RT and for (b) 6 h, (c) 8 h and (d) 10 h at 70 °C grown on Al <sub>2</sub> O <sub>3</sub> substrates.....	114
Figure 4.49: Raman spectra of SnO <sub>2</sub> thin films prepared from sol solution aging for 24 h at RT grown on different substrates. ....	115

Figure 4.50: Raman spectra of SnO <sub>2</sub> thin films prepared from sol solution aging for 6 h at 70 °C grown on different substrates.....	116
Figure 4.51: Raman spectra of SnO <sub>2</sub> thin films prepared from sol solution aging for 10 h at 70 °C grown on different substrates.....	117
Figure 4.52: The values of A <sub>1g</sub> mode versus annealing temperatures of NC SnO <sub>2</sub> thin films prepared from sol solutions aging at (a) for 24 h at RT and for (b) 6 h, (c) 8 h and (d) 10 h at 70 °C grown on Al <sub>2</sub> O <sub>3</sub> substrates. ....	119
Figure 5.1: Forward and reverse <i>I-V</i> measurements of Pd-NC SnO <sub>2</sub> -Pd contacts of the fabricated devices. ....	122
Figure 5.2: Cross-section FESEM micrographs of NC SnO <sub>2</sub> thin films grown on bare Si (100), SiO <sub>2</sub> /Si and Al <sub>2</sub> O <sub>3</sub> substrates.....	124
Figure 5.3: The sensitivity and repeatability of NC SnO <sub>2</sub> thin films gas sensor that was prepared from sol solution with glycerin grown on bare Si (100) substrates, aging for 8 h at 70 °C and annealed at 500 °C and upon exposure to successive pulses of 1000 ppm H <sub>2</sub> /N <sub>2</sub> gas and dry air at different sensor temperatures: (a) RT, (b) 75 °C and (c) 125 °C.....	126
Figure 5.4: The sensitivity and repeatability of NC SnO <sub>2</sub> thin films gas sensor, that was prepared from sol solution with glycerin grown on bare Si (100) substrates, aging for 10 h at 70 °C and annealed at 400 °C and upon exposure to successive pulses of 1000 ppm H <sub>2</sub> /N <sub>2</sub> gas and dry air at different sensor temperatures: (a) RT, (b) 75 °C and (c) 125 °C.....	127
Figure 5.5: The sensitivity of NC SnO <sub>2</sub> thin films gas sensor grown on bare Si (100) substrates, that was prepared from sol solution with glycerin aging for 8h at 70 °C and annealed at 500 °C under exposure to H <sub>2</sub> gas with different concentrations (150-1000) ppm at different sensor temperatures: (a) RT, (b) 75 °C and (c) 125 °C.....	128
Figure 5.6: The sensitivity of NC SnO <sub>2</sub> thin films gas sensor grown on bare Si (100) substrates, that was prepared from sol solution with glycerin aging for 10 h at 70 °C and annealed at 400 °C under exposure to H <sub>2</sub> gas with different concentrations (150-1000) ppm at different sensor temperatures: (a) RT, (b) 75 °C and (c) 125 °C.....	129
Figure 5.7: The sensitivity and repeatability of NC SnO <sub>2</sub> thin film sensor grown on SiO <sub>2</sub> /Si substrates upon exposure to successive pulses of 1000 ppm H <sub>2</sub> /N <sub>2</sub> gas and dry air at different sensor temperatures: (a) RT, (b) 75 °C and (c) 125 °C. ....	132
Figure 5.8: The sensitivity of NC SnO <sub>2</sub> thin film sensor grown on SiO <sub>2</sub> /Si substrates under exposure to different concentrations of H <sub>2</sub> (150-	

1000) ppm at different sensor temperatures: (a) RT, (b) 75 °C and (c) 125 °C. ....	134
Figure 5.9: The relationship between the sensitivity and operating temperatures for NC SnO <sub>2</sub> thin film sensor grown on SiO <sub>2</sub> /Si substrates in detecting 1000 ppm H <sub>2</sub> /N <sub>2</sub> gas and dry of H <sub>2</sub> gas. ....	134
Figure 5.10: The sensitivity and repeatability of NC SnO <sub>2</sub> thin film sensor grown on Al <sub>2</sub> O <sub>3</sub> substrates upon exposure to successive pulses of 1000 ppm H <sub>2</sub> /N <sub>2</sub> gas and dry air at various sensor temperatures: (a) RT, (b) 75 °C and (c) 125 °C.....	137
Figure 5.11: The sensitivity of NC SnO <sub>2</sub> thin film sensor grown on Al <sub>2</sub> O <sub>3</sub> substrates under exposure to H <sub>2</sub> gas with various concentrations (150-1000) ppm at various sensor temperatures: (a) RT, (b) 75 °C and (c) 125 °C. ....	138
Figure 5.12: The relationship between the sensitivity and operating temperatures for NC SnO <sub>2</sub> thin film sensor grown on Al <sub>2</sub> O <sub>3</sub> substrates in detecting 1000 ppm H <sub>2</sub> /N <sub>2</sub> gas and dry of H <sub>2</sub> gas. ....	139

## LIST OF SYMBOLS

$T$	Absolute temperature
$\text{\AA}$	Angstrom
$A$	Area of Schottky contact
$V$	Bias voltage
$K$	Boltzmann constant
$CB$	Conduction band
$D$	Crystallite size
$I_{air}$	Current in the presence gas
$I_g$	Current in the presence gas
$I-t$	Current- time
$I-V$	Current-voltage
$A^{**}$	Effective Richardson constant
$q$	Electron charge
$E_o$	Electron energy in vacuum
$E_g$	Energy Band gap
$E_f$	Fermi level
$B$	Full width at half maximum
$n$	Ideality factor
$d_{hkl}$	Inter-plane distance
$a, c$	Lattice constants
$\varepsilon_a$	Lattice strain
$hkl$	Miller indices
$I_o$	Saturation current
$\Phi_B$	Schottky barrier height



$X_o$	Semiconductor electron affinity
$S$	Sensitivity
$VB$	Valance band
$V$	Voltage
$\Phi$	Work function
$\lambda$	X-ray wavelength

## LIST OF ABBREVIATIONS

EDX	Energy-dispersive X-ray spectroscopy
FESEM	Field emission scanning electron microscope
FWHM	Full width at half maximum
MSM	Metal-semiconductor-metal
MBE	Molecular beam epitaxy
NC	Nanocrystalline
ppm	Part per million
PLD	Pulsed laser deposition
W	Saturated hydrogen electrode
SBH	Schootky barrier height
sccm	Standard cubic centimeters per minute
XRD	X-ray diffraction

**PENDERIA GAS HIDROGEN BERASASKAN SAPUT NIPIS  
NANOABLURAN SnO<sub>2</sub> DITUMBUHKAN DI ATAS SUBSTRAT BERBEZA  
MENGUNAKAN KAEDAH SALUTAN PUTARAN SOL-GEL**

**ABSTRAK**

Salutan putaran sol-gel adalah kaedah suhu rendah (di bawah 100 °C) dan berkemungkinan kaedah berkos paling rendah bagi pertumbuhan nanohabluran (NC) SnO<sub>2</sub> di atas pelbagai substrat. NC SnO<sub>2</sub> mempunyai potensi menambahbaik sifat-sifat penderiaan gas peranti juga secara ketara mengurangkan kos. Saput nipis SnO<sub>2</sub> sedia endap dan disepuh lindap mengalami keretakan yang muncul dpermukaan SnO<sub>2</sub> dan mempamerkan kesan tindak balas negatif ke atas prestasi peranti. Oleh itu, nisbah isipadu berbeza bagi gliserin (0:1, 1:12, 1:8) telah ditambah kepada larutan sol bagi mengatasi masalah keretakan. Saput nipis NC SnO<sub>2</sub> ditumbuh di atas tiga substrat yang berbeza iaitu, Si (100) tanpa salutan, SiO<sub>2</sub>/Si dan Al<sub>2</sub>O<sub>3</sub>. Mekanisma pertumbuhan NC SnO<sub>2</sub> disiasat melalui pembelauan sinar-X (XRD), mikroskop imbasan elektron medan pancaran (FESEM), spektroskopi sebaran tenaga sinar-X (EDX) dan spektroskopi Raman. Nisbah isipadu gliserin terbaik ialah (1:12) yang menyingkirkan keretakan dan menambahbaikkan penghabluran. Analisis pembelauan sinar-X menunjukkan sifat amorfus bagi saput nipis sedia endap. Sampel yang disepuh lindap pada suhu 400 °C selama 2 jam dalam udara mempamerkan puncak pantulan yang bersetuju dengan struktur rutil tetragonal bagi SnO<sub>2</sub> pukal piawai. Meningkatkan suhu sepuh lindap dari 400 ke 600 °C telah menambahbaikkan penghabluran dan meningkatkan saiz habluran. Di samping itu, pengurangan dalam keterikan dan kecacatan hablur yang tercetus semasa penumbuhan lapisan seperti perkehelan yang berpunca daripada ketaksempurnaan larutan dehidrasi timah klorida di dalam larutan etanol tulen. Namun, imej FESEM menunjukkan pembentukan

aglomeratan di permukaan saput nipis NC SnO<sub>2</sub> apabila sampel disepuh lindap pada suhu 600 °C. Oleh kerana itu, larutan sol didedahkan dengan masa haba penuaan berbeza (24 jam pada suhu bilik (RT), dan 6, 8 dan 10 jam pada suhu 70 °C). Daripada pemerhatian EDX, apabila masa haba penuaan meningkat bersama peningkatan suhu sepuh lindap, kepekatan unsur bendasing klorin (Cl) dan karbon (C) menurun secara mendadak manakala kepekatan elemen Sn dan O meningkat. Mod getaran A<sub>1g</sub> bagi NC SnO<sub>2</sub> menunjukkan anjakan biru yang lemah dengan peningkatan masa haba penuaan berbanding dengan anjakan biru yang ketara dengan peningkatan suhu penyepuh lindapan. Keputusan ini menunjukkan bahawa penghabluran tinggi saput nipis SnO<sub>2</sub> tanpa aglomeratan di atas substrat SiO<sub>2</sub>/Si dan Al<sub>2</sub>O<sub>3</sub> terjadi bagi larutan sol dengan penuaan 8 jam pada 70 °C dan sampel disepuh lindap pada 500 °C. Bagi saput nipis SnO<sub>2</sub> yang ditumbuhkan di atas Si (100) tanpa salutan, masa penuaan larutan sol yang terbaik ialah 8 dan 10 jam pada 70 °C dengan suhu sepuh lindap masing-masing pada 500 °C dan 400 °C. Peranti pengesan gas hidrogen logam-semikonduktor-logam (MSM) telah dihasilkan melalui pengendapan penyentuh palladium (pd) di atas permukaan selaput nipis NC SnO<sub>2</sub>. Ciri-ciri sentuhan *I-V* Schottky bagi semua penderia gas, telah diukur pada RT. Sifat penderiaan bagi gas H<sub>2</sub> adalah bolehulang meliputi masa ujian (50 min) bagi kepekatan gas H<sub>2</sub> yang berbeza pada suhu operasi yang berbeza. Penambahan gliserin ke larutan sol meningkatkan keliangan pada permukaan NC SnO<sub>2</sub>, apabila sampel terdedah kepada penyepuhlindapan di atas takat didih gliserin, yang mana penyejatan gliserin itu membawa kepada penghasilan lompong, yang menjana nisbah kawasan permukaan kepada isipadu yang tinggi. Akibatnya, keadaan ini membenarkan proses penyerapan/penyahnyerapan molekul H<sub>2</sub> dan O<sub>2</sub> di atas permukaan saput nipis NC SnO<sub>2</sub>, yang menambahbaik kepekaan peranti yang telah

difabrikasi. Kepekaan bagi penderia pertama dan kedua yang ditumbuhkan di atas substrat Si (100) tanpa salutan masing-masing adalah 120% dan 90%, dengan kehadiran 1000 ppm H<sub>2</sub>/ disambungkan dengan N<sub>2</sub> dan udara kering. Kepekaan penderia yang difabrikasi di atas substrat SiO<sub>2</sub>/Si meningkat ke 600%, dan kepekaan penderia yang difabrikasi di atas substrat Al<sub>2</sub>O<sub>3</sub> meningkat sehingga ke 2570% bagi kepekatan gas yang sama. Tambahan lagi, keboleholangan dan kepekaan dipertingkatkan dengan peningkatan suhu operasi. Nilai kepekaan peranti pengesanan gas H<sub>2</sub> berdasarkan selaput nipis NC SnO<sub>2</sub> yang ditumbuhkan pada substrat Al<sub>2</sub>O<sub>3</sub> mengatasi peranti rekaan lain dan menunjukkan prestasi yang tinggi untuk mengesan perbezaan kepekatan H<sub>2</sub> (150-1000 ppm) pada suhu yang berbeza (suhu bilik, 75 dan 125 °C) .

**HYDROGEN GAS SENSORS BASED ON NANOCRYSTALLINE SnO<sub>2</sub> THIN  
FILMS GROWN ON DIFFERENT SUBSTRATES USING SOL-GEL SPIN  
COATING METHOD**

**ABSTRACT**

Sol-gel spin coating is a low-temperature method (below 100 °C) and possibly the lowest cost method for growing nanocrystalline (NC) tin dioxide (SnO<sub>2</sub>) on various substrates. NC SnO<sub>2</sub> has potential to improve the properties of gas sensor device while also significantly lowering the cost. As-deposited and annealed SnO<sub>2</sub> thin films suffered from cracks that appeared on the surface of the SnO<sub>2</sub> thin films and they exhibited negative response effects of device performance. Therefore, different volume ratios of glycerin (0:1, 1:12 and 1:8) are added to the sol solutions to overcome the problem of cracks. NC SnO<sub>2</sub> thin films are grown on three different substrates, namely, bare silicon Si (100), silicon dioxide SiO<sub>2</sub>/Si, and sapphire Al<sub>2</sub>O<sub>3</sub>. The growth mechanisms for the NC SnO<sub>2</sub> are investigated through X-ray Diffraction (XRD), field emission scanning electron microscope (FESEM), Energy Dispersive X-ray spectroscopy (EDX) and Raman spectroscopy. The best glycerin volume ratio determined is (1:12), which eliminated cracks and improved the crystallization. X-ray diffraction analysis indicated the amorphous nature of the as-deposited thin films. The samples annealed at 400 °C for 2 h in air exhibited reflection peaks that agreed with the tetragonal rutile structure of standard bulk SnO<sub>2</sub>. Increasing annealing temperatures from 400 to 600 °C resulted in improvement in the crystallization and increase in the crystallite size. In addition, we observed a reduction of strains and crystalline defects induced during growth of the film such as dislocations, which originated from the incomplete dissolving of tin (II) chloride dihydrate in pure ethanol. However, FESEM images showed the formations of

agglomeration on the surface of NC SnO<sub>2</sub> thin films when the samples were annealed at 600 °C. Therefore, the sol solutions were exposed to different aging heat times (24 h at room temperature (RT) and for 6, 8 and 10 h at 70 °C). For the EDX observation, when aging heat time increased in the presence of increasing annealing temperatures, the impurity concentrations of chlorine (Cl) and carbon (C) elements decreased sharply while the concentrations of Sn and O elements increased. The A<sub>1g</sub> modes of the NC SnO<sub>2</sub> showed a weak blue shift with increasing aging heat times as compared with a noticeable blue shift with increasing annealing temperatures. The results showed that the high crystallization for SnO<sub>2</sub> thin films without agglomerations on SiO<sub>2</sub>/Si and Al<sub>2</sub>O<sub>3</sub> substrates occurred for sol solution time of 8 h at 70 °C and the samples annealed at 500 °C. For the SnO<sub>2</sub> thin films grown on bare Si (100), the best sol solution aging times are 8 and 10 h at 70 °C at annealing temperatures of 500 °C and 400 °C, respectively. Metal-semiconductor-metal (MSM) hydrogen (H<sub>2</sub>) gas sensor devices have been fabricated through the deposition of palladium (Pd) contacts on the top surface of NC SnO<sub>2</sub> thin film. The *I-V* characteristics of all the gas sensors are observed at RT. The sensing properties of H<sub>2</sub> gas sensor are repeatable over the test time (50 min) for different H<sub>2</sub> gas concentrations at different operating temperatures. The addition of glycerin to sol solutions increased the porosity of NC SnO<sub>2</sub> film when the sample is exposed to an annealing temperature above the boiling point of glycerin, of which the evaporation of glycerin leads to a production of voids, which provide a high surface-area to volume ratio. Consequently, this condition allowed for easy adsorption/desorption processes of H<sub>2</sub> and oxygen (O<sub>2</sub>) molecules on the NC SnO<sub>2</sub> films surface, which improved the sensitivity of fabricated devices. The sensitivity of the first and the second sensors grown on bare Si (100) substrates are 120% and 90%, respectively, in the presence of

1000 ppm H<sub>2</sub>/ balanced N<sub>2</sub> and dry air. The sensitivity of the sensor fabricated on SiO<sub>2</sub>/Si substrate increased to 600%, and the sensitivity of the sensor fabricated on Al<sub>2</sub>O<sub>3</sub> substrates increased by up to 2570% for the same gas concentrations. Furthermore, the repeatability and sensitivity are enhanced with increasing operating temperatures. The sensitivity value of H<sub>2</sub> gas sensor device based on NC SnO<sub>2</sub> thin film grown on Al<sub>2</sub>O<sub>3</sub> substrate outperformed other fabricated devices and showed high performance for detection different H<sub>2</sub> concentrations (150–1000 ppm) at different operating temperatures (room temperature, 75 and 125 °C).



# CHAPTER 1

## INTRODUCTION

### 1.1 Overview

High performance gas sensors have received great attention because of their importance in various fields, especially in chemical industries, safety systems, environmental monitoring and chimerical flame detection [1, 2]. Tin dioxide ( $\text{SnO}_2$ ) displays versatile characteristics such as chemical sensitivity to several gases, high chemical stability, low cost and flexibility in fabrication [3, 4]. Furthermore,  $\text{SnO}_2$  can be potentially applied in other applications such as thin film electroluminescent displays, solar cells and heat reflectors [5, 6].

$\text{SnO}_2$  based gas sensor is commonly studied because of its wide direct band gap ( $\sim 3.6$  eV) at 300 K as well as  $\text{SnO}_2$  is an n-type semiconductor that has a tetragonal rutile structure [7-10]. Metal oxide-semiconductor exhibits sensitivity to a variety of gases in the atmosphere because of variation in their electrical characteristics [11].  $\text{SnO}_2$  dominates over of all other metal oxide-semiconductors and is the most widely used in the gas sensor field because of its many advantages such as low cost fabrication, higher sensitivity, thermal stable structure and low operating temperature [12]. In 1971, Naoyshi successfully fabricated and patented the first gas sensor device for practical applications using  $\text{SnO}_2$  as the sensitive material [13]; since then, studies on  $\text{SnO}_2$  gas sensors have been extensively developed.  $\text{SnO}_2$  has been successfully used to detect various gases, including hydrogen ( $\text{H}_2$ ), hydrogen sulfide ( $\text{H}_2\text{S}$ ), nitrogen dioxide ( $\text{NO}_2$ ), carbon monoxide ( $\text{CO}$ ), oxygen ( $\text{O}_2$ ), methanol ( $\text{CH}_4\text{O}$ ) and ammonia ( $\text{NH}_3$ ) [14-18].

In the current global economy, H<sub>2</sub> has become an important subject for the development of new sustainable energy because it is an efficient and clean energy source that is widely used as replacement of oil in automobiles, aircraft, fuel cells, and chemical industries [19, 20]. H<sub>2</sub> is an odorless, colorless and highly volatile, inflammable and explosive gas when its concentration in dry air is beyond 4% [20]. Consequently, H<sub>2</sub> gas sensors that show good performance at room temperature (RT) are highly required in the chemical industries and in environment applications to detect the formation of potentially explosive mixtures with air. Therefore, the gas sensors help prevent the risks of explosions and fires [21-23]. Moreover, H<sub>2</sub> gas sensors operate at RT that have numerous benefits such as low power consumption and cost-effective [21, 24], ability to be used safely in inflammable and toxic gases [25] and long lifetime [26].

The improvement of the gas sensing properties for the SnO<sub>2</sub> nanostructure is affected by several factors such as morphology, operating temperature, adsorption/desorption process and porosity for sensor design. The control on the gas parameters improves the sensitivity and selectivity of nanocrystalline (NC) SnO<sub>2</sub> sensors. These improvements are achieved by enhancement of film porosity, tuning of annealing temperature, and the modulation of the sensor operating temperature [27, 28]. The Schottky contact formation is an effective method to obtain a large barrier height in the metal-semiconductor (MS) contact for high performance gas sensors.

## **1.2 Motivations and problem statements**

SnO<sub>2</sub> nanostructures can be prepared by several methods such as sol-gel spin coating [29], pulsed laser deposition (PLD) [30], hydrothermal [31], molecular beam epitaxy (MBE) [32] and thermal evaporation [33]. The sol-gel spin coating method

has been selected for the preparation of NC SnO<sub>2</sub> thin films because of its several advantages compared with other methods. This method is operated at low reaction temperatures, easy to process and not expensive. The film thickness can also be easily changed by changing either the spin speed or the viscosity [34].

Thin films deposited onto different substrates through the sol–gel spin coating method suffer from cracks problem at RT and at different annealing temperatures. Cracks occurred when the liquid evaporates from the gels during the drying processes, which result in gel shrinkage [35]. Glycerin can be added to the sol solution to overcome these cracks [36]. Therefore, a study on the effect of adding glycerin to the sol solutions with different volume ratios is required to select the best volume ratio of glycerin that should be added to the sol solution. Determining this volume ratio can eliminate cracks problem, in which glycerin contains three hydroxyl groups that can produce hydrogen bonds with other atoms [37, 38], and could contribute to improving the characterization. Through enhanced dissolving of tin (II) chloride dihydrate in pure ethanol and the formation of voids during glycerin evaporation, the porosity of the surface of the nanocrystalline (NC) SnO<sub>2</sub> thin film increases, thereby providing a high surface-area to volume ratio. Other factors such as increasing the aging heat times of sol solutions and annealing temperature can enhance the crystallization of SnO<sub>2</sub> thin films that are produced by sol- gel spin coating method.

Several factors can improve the crystallization of SnO<sub>2</sub> thin films such as aging heat times and annealing temperatures, but can also generate agglomerations, wherein the nanoparticles can be clumped together. These agglomerations are undesirable because they decrease the performance of the devices. Consequently, a study on the effects of aging heat times and annealing temperatures is necessary to

select the best crystallization of the SnO<sub>2</sub> thin films without agglomerations. Generally, gas sensing tests are carried out at high operation temperatures. SnO<sub>2</sub> thin film H<sub>2</sub> gas sensor indicated low performance when tested at operation temperature near to RT. Therefore, different substrates are used to determine the best crystallization parameters and low fabrication cost of NC SnO<sub>2</sub> thin films, which can improve the sensitivity of the gas sensor.

### **1.3 Scope of study**

This study focuses on the growth of SnO<sub>2</sub> thin films on bare silicon [Si (100)], silicon dioxide (SiO<sub>2</sub>) layer formed on Si(100) substrate (SiO<sub>2</sub>/Si) and sapphire (Al<sub>2</sub>O<sub>3</sub>) substrates at low temperature using the sol-gel spin coating method. Studying the effect of adding glycerin at different volume ratios (0:1, 1:12 and 1:8) to the sol-solutions on the characterizations of NC SnO<sub>2</sub> thin films. Selecting the best values for different aging heat time and annealing temperature is specified to avoid the formation of agglomerations and to produce high quality NC SnO<sub>2</sub> without cracks and agglomerations. Therefore, the sol solutions exposed to different aging heat times (24 h at RT, and for 6, 8 and 10 h at 70 °C), and the as-deposited thin films exposed to different annealing temperatures (400, 500 and 600 °C) are investigated. The structural properties and surface morphology of thin films are analyzed by X-ray diffraction (XRD), field emission scanning electron microscope (FESEM), energy dispersive X-ray spectroscopy (EDX) and Raman spectroscopy. The optimized NC SnO<sub>2</sub> thin films deposited on different substrates are selected to fabricate gas sensors, which showed a high ability to detect H<sub>2</sub> gas when exposed to different concentrations of H<sub>2</sub> at different operating temperatures.

#### **1.4 Objectives of the research**

The main objectives of this research are as follows:

1. To prepare high quality NC SnO<sub>2</sub> thin films without cracks through the sol-gel spin coating method by investigating the best volume ratio of glycerin that should be added to the sol solutions.
2. To obtain the optimal growth and high characterization of NC SnO<sub>2</sub> thin films without agglomerations by exploring the best values of aging heat time and annealing temperature at a constant volume ratio of glycerin.
3. To fabricate metal-semiconductor-metal (MSM) H<sub>2</sub> gas sensors based on optimized NC SnO<sub>2</sub> thin films on (bare Si (100), SiO<sub>2</sub>/Si and Al<sub>2</sub>O<sub>3</sub>) substrates, which can show good detector performance at different operating temperatures, especially at RT for different gas concentrations.
4. To improve H<sub>2</sub> gas sensor performance, especially at RT as well as increase the sensitivity and stability by enhancing the process of adsorption/desorption of gas molecules.

#### **1.5 Originality of the research**

This research provides the following originality to solve the problems presented in Section 1.2:

- 1- Selection of the best glycerin volume ratio that should add to the sol solutions to eliminate cracks problem, enhance the crystallization and increase surface porosity.
- 2- Selection of the best value of aging heat time and annealing temperature that can be produced high quality NC SnO<sub>2</sub> thin films without agglomerations.

- 3- Fabrication H<sub>2</sub> gas sensors based on NC SnO<sub>2</sub> thin films grown on bare Si (100) substrates that can be operated at RT, 75 and 125 °C.
- 4- Fabrication of gas sensors based on NC SnO<sub>2</sub> thin film grown on SiO<sub>2</sub>/Si and Al<sub>2</sub>O<sub>3</sub> substrates with high detection ability for different H<sub>2</sub> gas concentrations at operating temperatures (RT, 75 and 125 °C).

## 1.6 Outline of the research

The organization of the present study is as follows:

**Chapter 1** introduces a brief overview of SnO<sub>2</sub> nanostructures, motivations and problem statements, scope of study, objectives and finally the originality of this research.

**Chapter 2** provides a literature review for growth of SnO<sub>2</sub> nanostructures and gas sensors based on SnO<sub>2</sub> nanostructures. In addition, the sol-gel spin coating method is also presented. The theoretical background of the structural properties of SnO<sub>2</sub>, surface properties, metal-semiconductor (MS) contact, gas sensing properties and sensing mechanism of SnO<sub>2</sub> nanostructures are discussed.

**Chapter 3** presents the details of methodology and instruments systems that used to prepare and measure the NC SnO<sub>2</sub> thin films, as well as introduces the fabrication steps and gas sensing system of the MSM H<sub>2</sub> gas sensors.

**Chapter 4** discusses the results of the preparation and characterization of SnO<sub>2</sub> thin films grown on bare Si (100), SiO<sub>2</sub>/Si and Al<sub>2</sub>O<sub>3</sub> substrates that exposed to different growth parameters.

**Chapter 5** focuses on the current-voltage *I-V* characteristics of the fabricated sensors based on NC SnO<sub>2</sub> that have been grown on bare Si (100), SiO<sub>2</sub>/Si and Al<sub>2</sub>O<sub>3</sub> substrates. The performance of these sensors when exposed to different H<sub>2</sub>

gas concentrations at different operating temperatures is also discussed.

Finally, **Chapter 6** presents the conclusions of the study and possible future works.

## CHAPTER 2

### LITERATURE REVIEW AND THEORETICAL BACKGROUND

#### 2.1 Introduction

Several studies have been conducted on the use of SnO<sub>2</sub> as a gas sensor because of its large band gap, thermal stability and low cost. This chapter presents a summary and literature review of the previous studies performed on the preparation of SnO<sub>2</sub> nanostructure, the structural characteristics, surface morphology investigations, and gas sensing properties. The factors that could contribute to the improvement of the performance of the fabricated SnO<sub>2</sub> nanostructure sensor are discussed. Moreover, this chapter also discusses the theoretical background of the tetragonal rutile structure of SnO<sub>2</sub> thin films; basic equations and issues related to metal-semiconductor contact and gas sensing behaviour.

#### 2.2 Nanomaterials

In the last two decades, nanoscience and nanotechnology have been vital subjects because of their use in different applications such as gas sensor devices, photodetectors and solar cells. Nanomaterials exist in a dimension of less than 100 nm [39]. Nanostructured materials can be classified into four types comprising 0-dimensional (0D) (quantum dots, nanoparticles, etc.), 1-dimensional (1D) (nanotubes, nanorods and nanowires), 2-dimensional (2D) (thin films and nanosheets) and 3-dimensional (3D) (nanospheres). Nanomaterials are crucial in modern applications because of their unique physical and chemical characteristics.



Several methods can be used to prepare the nanostructured materials. These methods involve the liquid phase methods, mixed phase syntheses and gas phase methods. Selection on a suitable method is significant to determine the failure or success of the prepared nanostructured materials, due to their physical and chemical characteristics, and the applications of nanomaterials are powerfully reliant on how they are fabricated. Moreover, the significance of choosing a suitable method in forming nanomaterials has been a motivating force for the development of new methodologies.

### **2.3 Literature review for the growth of SnO<sub>2</sub> nanostructures and gas sensors based on SnO<sub>2</sub> nanostructures**

#### **2.3.1 Growth of SnO<sub>2</sub> nanostructures**

Generally, SnO<sub>2</sub> nanostructures can be prepared using different methods on different types of substrates such as sol-gel spin coating, thermal evaporation, chemical precipitation, PLD and hydrothermal methods. As well as SnO<sub>2</sub> nanoparticles powders can be prepared without substrates by sol-gel method. These methods produce different growth morphologies such as nanoparticles, nanowires, nanobelts, nanospheres, nanosheet and NC SnO<sub>2</sub> thin films [40, 41].

#### **2.3.2 Sol-gel spin coating method**

Sol-gel spin coating method has been used to produce uniform thin films on flat substrates, which have several benefits, such its ability to operate at low reaction temperatures, relatively low cost and easy process [42]. This method was used in the 1950s by Larson and Rehg when they deposited phosphor on the glass surfaces of color television tubes [43].

At the beginning, sol solution should be prepared by dissolving the source of material, which is usually a salt material in a suitable solvent. These solvents depend on the type of source material, which should be one of water, organic material, acidic or alkaline substance. For example, the suitable solvent for dissolving tin (II) chloride dihydrate ( $\text{SnCl}_2 \cdot 2\text{H}_2\text{O}$ ) is ethanol ( $\text{C}_2\text{H}_5\text{OH}$ ) [36]. Practically, the precursor solution is stirred using a magnetic stirrer at the appropriate temperature for times ranging from 1 to 24 h to achieve good dissolving ability for the source of material in the solvent [44, 45].

Figure 2.1 (a) shows the spin coating system used to deposit the sol-gel solution based on different types of substrates. The mechanism of spin coating process can be divided into four steps [46, 47]. The first step is dropping the solution on the center of the substrate using a micropipette. The second step is to accelerate the substrate gradually until it reaches to the desired final spin speed. In this step, the spin speed increases by increasing the centripetal acceleration and some amount of solution will be ejected from the edge of the substrate. The third stage starts when the substrate spins with a constant spin speed and the net solution that flows from the edge of the substrate becomes negligible and viscous forces dominate solution thinning behavior and its attachment on the substrate [48, 49], as shown in Figure 2.1 (b),

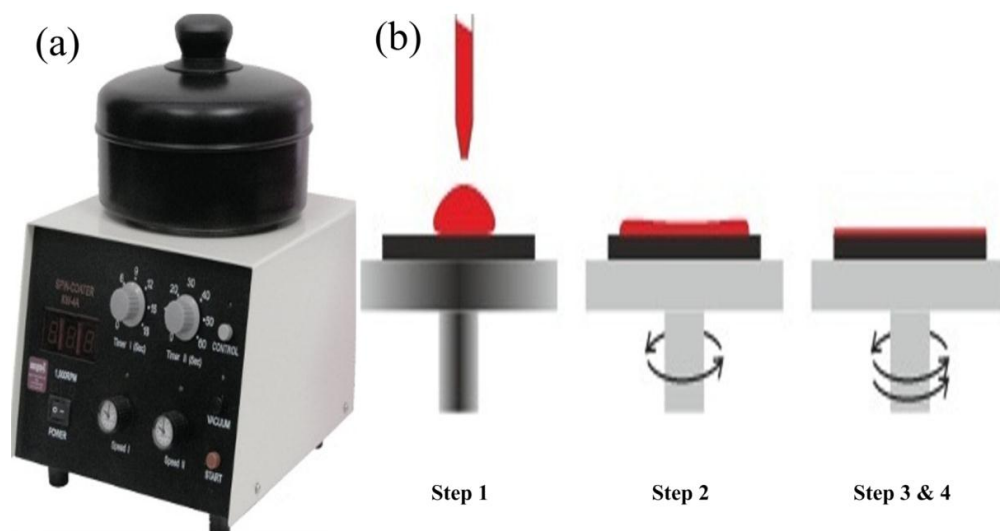


Figure 2.1: Spin coating process (a) spin coating system, (b) the four steps involved [50].

Finally, the fourth step begins during the spin-off when the spin speed of the substrate decreases gradually until it stops. During the spin-off, the substrate still spins, but the centrifugal outflow stops and further thinning of film occurs because of solvent evaporation. Then, the as-deposited thin film dried in an oven at a suitable temperature depending on the evaporation temperature of the solvent which ranging from 10 to 30 min [51] In addition, the vacuum pump device is part of the spin coating system that creates a vacuum and holds the film tightly to prevent it from slipping and breaking [52]. Spin speed should be slow to reduce the ejected amount of solution from the edge of the substrate in the second step. Thus, two spin speeds are used. The first spin speed should be slow, reaching approximately 500– 900 rpm, and last only for several seconds (applied in the second step). The second spin speed should be higher than the first spin speed, reach approximately 1500–5000 rpm, and last for a longer time to approximately 10–70 s (applied in the third step).

Film thickness depends on the nature of the sol solution such as viscosity, drying rate, percent solids (the concentration of material source) and surface tension.

Spin process factors can influence in the thickness of film such as spin speed, acceleration, amount of the delivered solution and spin time. Practically, the spin speed increases with increasing viscosity of solution. Fast spin speed and long spin time create thinner film [34]. The spin coating and drying operations should be repeated many times to increase the thickness of film [53].

Liu et al. [36] synthesized SnO<sub>2</sub> thin films on Al<sub>2</sub>O<sub>3</sub> substrates through sol-gel spin coating method; the as-deposited thin films were amorphous. The samples were sintered in air at 550 °C for 2 h in order to obtain the crystallization of SnO<sub>2</sub> films. Glycerin was added to the sol solution to eliminate cracks. In addition, they studied the effect of cooling rate at 1800, 200, 100 and 25 °C/h and found the crystallite size was  $21 \pm 0.4$  nm. Thus, they concluded that the cooling rate caused by the limitation influence on crystallite size of thin films, where the crystallites of SnO<sub>2</sub> ceases to grow up under the cooling process. Kose et al. [54] used the same method to synthesize SnO<sub>2</sub> thin films on glass substrates. The crystallization of thin films was achieved after the samples calcined in air at temperature reaching 600 °C at a heating rate of 2 °C /min. The formations of agglomerations were observed on the surface of films due to the increase of ethanol ratio with reduced glycerin ratio in the precursor solution that produced roughness of SnO<sub>2</sub> thin films. The adding glycerin leads to enhance film porosity and increased solution viscosity. XRD analysis indicated that the broadest (110) peak occurred because of the nanoparticles size became very small.

Sakai et al. [55] prepared SnO<sub>2</sub> thin films using spin coating method from a hydrothermal sol suspension on Al<sub>2</sub>O<sub>3</sub> substrates. The samples were sintered at 600 °C for 3 h in air to obtain the crystallization of SnO<sub>2</sub> thin films. SnO<sub>2</sub> films with

thicknesses over 300 nm were selected and used to fabricate gas sensor devices. These thin films were selected because the cracks did not penetrate through the film down toward the bottom. The thickness of films increased steeply with increasing spin coating times. It was also found that the thickness of SnO<sub>2</sub> thin films ranged from 100 to 300 nm but the average size of grain was still of 6 nm on average.

Cha et al. [56] used spin coating method for the deposition of the washed gel of SnO<sub>2</sub> thin films on alumina substrate. Calcination temperatures affected grain size, morphology and microstructure of the films. XRD analysis showed improved crystallinity of SnO<sub>2</sub> thin films and increased grain size after increasing the calcination temperature from 500 to 900 °C. Surface morphology analysis demonstrated that cracks appeared on the surface of the films at different calcination temperatures and became larger at high calcine temperatures. This phenomenon decreased the stability of the mechanical attributes. Agglomerations also occurred in the grains during calcination.

Similar results were obtained by Esfandyarpour et al. [29] for SnO<sub>2</sub> thin films deposited on Si (100) substrates using sol-gel spin coating method. Superficial cracks appeared on the surface of SnO<sub>2</sub> films during calcination. However, they assumed that the superficial cracks did not penetrate via the film down to the bottom. Jeng [57] found that the as-deposited SnO<sub>2</sub> thin films on quartz glass substrates prepared by sol-gel spin coating method was amorphous. The crystallization of thin films was enhanced with increased annealing temperature in O<sub>2</sub> gas and in N<sub>2</sub> gas. SEM morphology showed a smooth surface for the as-deposited thin films. However, small nodules appeared on the surface of SnO<sub>2</sub> thin films after the films were annealed. Surface morphology changed from small to large nodules after annealing

temperature was increased from 300 to 500 °C. Izydorczyk et al. [58] successfully deposited SnO<sub>2</sub> thin films on SiO<sub>2</sub>/Si substrates through sol-gel spin coating method. The crystallization and the diameter of nano-grains for different molar concentrations of the sol solution increased with increased annealing temperatures from 700 to 900 °C.

Similar method was used by Uysal and Arier [59] to prepare SnO<sub>2</sub> nano films on glass substrates with different concentration of water. They found that the crystallite size of SnO<sub>2</sub> increased from 6 to 22 nm with increasing annealing temperatures from 450 to 650 °C at volume ratio 1: 0.025 of SnCl<sub>2</sub>: water.

Shoyama et al. [60] used same method to show that the addition of poly ethylene glycol (PEG) avoided the agglomerations of SnO<sub>2</sub> particles, which were deposited on Si (100) substrates. The topography images indicated that 3.3 wt.% of PEG is necessary to prevent the particle agglomerations of the SnO<sub>2</sub> particles, while the agglomerations of SnO<sub>2</sub> particles occurred in the PEG-free SnO<sub>2</sub> thin films. Furthermore, the thickness of the annealed thin films at 500 °C with the presence PEG 3.3 wt.% was around 600 nm and the particle size decreased from 30 to 10 nm after PEG was added to the sol solution. XRD analysis showed that the crystallinity of SnO<sub>2</sub> thin films improved with increased annealing temperatures from 500 to 800 °C.

Kaur et al. [61] used the same method to deposit SnO<sub>2</sub> nanoparticles on the float glass substrates. The degradation in the performance of the sensor based on these SnO<sub>2</sub> nanoparticles was noticed because of the agglomerations grown among nanoparticles. Indium-doped SnO<sub>2</sub> thin films with two different concentrations (5 wt% and 10 wt%) were used to resolve the problem of agglomerations of particles.

XRD analysis indicated that the full width at half maximum (FWHM) increased with increased in indium concentration in the SnO<sub>2</sub> films, thus, crystallite size decreased. Transmission electron microscope (TEM) micrographs demonstrated that the indium-doped SnO<sub>2</sub> thin films at concentration 10 wt% was suitable to prevent the problem of agglomerations of particles. Table 2.1 provides a list of NC SnO<sub>2</sub> thin films that were prepared by sol-gel spin coating method based on different types of substrates.

Table 2.1: Summary of the NC SnO<sub>2</sub> thin films prepared using sol-gel spin coating method.

Starting Materials	Substrates	Ref.
Tin (II) chloride dehydrate (SnCl <sub>2</sub> .2H <sub>2</sub> O), ethanol (C <sub>2</sub> H <sub>5</sub> OH) and glycerin (C <sub>3</sub> H <sub>8</sub> O <sub>3</sub> )	Al <sub>2</sub> O <sub>3</sub>	[36]
Tin chloride (SnCl <sub>4</sub> ), alcohol (C <sub>3</sub> H <sub>8</sub> O) chloroplatinic acid (H <sub>2</sub> Cl <sub>6</sub> Pt.6H <sub>2</sub> O)	Si (100)	[29]
Tin chloride pentahydrate (SnCl <sub>4</sub> .5H <sub>2</sub> O), antimony(III) acetate [Sb(OAC) <sub>3</sub> ] and ethanol (C <sub>2</sub> H <sub>5</sub> OH)	Quartz glass	[57]
Tin chloride pentahydrate (SnCl <sub>4</sub> .5H <sub>2</sub> O), and isopropanol (C <sub>3</sub> H <sub>8</sub> O)	SiO <sub>2</sub> /Si	[58]
Tin chloride (SnCl <sub>2</sub> ), 2-methoxyethanol CH <sub>3</sub> OC <sub>2</sub> H <sub>4</sub> OH and poly ethylene glucol (PEG)	Si (100)	[60]
Tin chloride pentahydrate (SnCl <sub>4</sub> .5H <sub>2</sub> O), ethanol (C <sub>2</sub> H <sub>5</sub> OH), water (H <sub>2</sub> O) and indium chloride (InCl <sub>3</sub> )	Float glass	[61]

### **2.3.3 Growth mechanism of SnO<sub>2</sub> thin films using sol-gel spin coating method**

SnO<sub>2</sub> thin films can be prepared using sol-gel spin coating method operated at low reaction temperatures (below 100 °C) by dissolving tin (II) chloride dihydrate (SnCl<sub>2</sub>·2H<sub>2</sub>O) in pure ethanol (C<sub>2</sub>H<sub>5</sub>OH) for a few hours. Therefore, a solution containing compounds of tin (II) chloride (SnCl<sub>2</sub>) and tin (II) hydroxide (Sn(OH)<sub>2</sub>) is produced. This solution can be deposited on different substrates using spin coating system. Then, when the samples are exposed to anneal in air, the hydrogen atoms will start to be removed, chloride will evaporate and be replaced by oxygen atoms [38]. Given that the material tends toward stability, the oxygen atom creates a double bond with tin to produce tin dioxide (SnO<sub>2</sub>); thus, the tin turn to tetravalent tin (IV).

Murugadoss et al. [62] found that, when SnCl<sub>2</sub> dissolved in the water solvent, uncontrolled Sn(OH)<sub>2</sub> nanoparticles may grow in the solution. That Sn(OH)<sub>2</sub> containing solution was deposited on a glass substrate and then annealed in air at 200 °C for 2 h, resulting in the formation of inhomogeneous SnO<sub>2</sub> nanoparticles by rapid oxidation.

The as-deposited and annealed SnO<sub>2</sub> thin films suffer from cracks [63]. Gawel et al. [35] suggested that the cracks are generated due to the evaporation of the liquid from the gels during drying, which can cause gel shrinkage.

### **2.3.4 Glycerin as binding agent**

Glycerin (C<sub>3</sub>H<sub>8</sub>O<sub>3</sub>) is a colorless, odorless, viscous liquid and completely soluble in water and alcohol, the boiling point is 290 °C. Glycerin can be used to remove cracking during the drying processes of the gels [35]. This may be due to the existence of three hydroxyl groups that produce hydrogen bonds with a pair of acceptors (chlorine and oxygen), and donor (hydrogen) atoms [37, 38]. Therefore,



glycerin can prevent cracks through the physical interaction between the hydrogen atoms of hydroxyl group of glycerin and the two compounds  $\text{SnCl}_2$  and  $\text{Sn}(\text{OH})_2$  as shown in Figure 2.2.

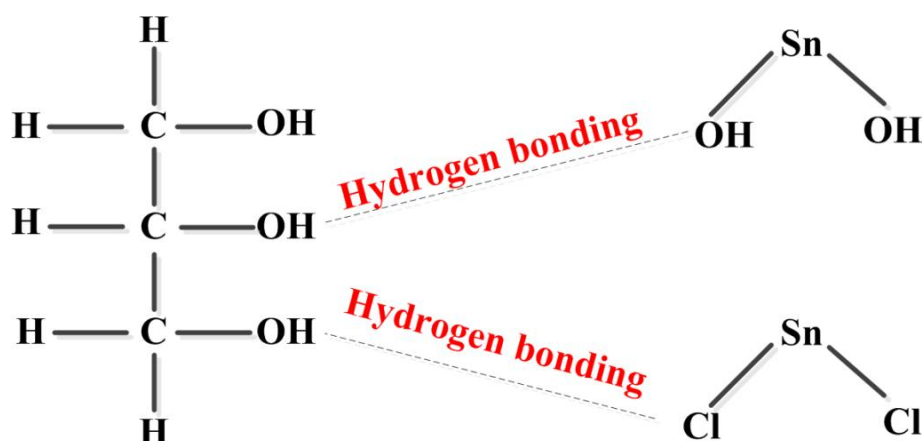


Figure 2.2 : Hydrogen bonding between glycerin and the compounds of  $\text{SnCl}_2$  and  $\text{Sn}(\text{OH})_2$ .

The solution can be deposited on different substrates and is exposed to air for annealing to obtain the  $\text{SnO}_2$  thin films as explained in section 2.3.3. During the annealing step to a temperature above its boiling point, glycerin, similar to any organic compound, will turn to carbon dioxide ( $\text{CO}_2$ ) and water vapor ( $\text{H}_2\text{O}$ ) [64]. Therefore, voids will be formed after the removal of glycerin, leading to enhanced porosity of the annealed samples. Kose et al.[65] mentioned that the addition of glycerin leads to enhanced film porosity.

A diol such as methanediol ( $\text{H}_2\text{C}(\text{OH})_2$ ) with two hydroxyl groups can be a replacement for glycerin, however it dissolved only in water not in ethanol, thus glycerin is preferred.

### 2.3.5 $\text{SnO}_2$ morphology changes with annealing temperature

The annealing temperature is an important parameter that affect the surface morphology of  $\text{SnO}_2$ . The surface of the as-deposited thin film prepared using sol-

gel spin coating method exhibits a smooth and continuous morphology, as is in agreement with the amorphous nature of SnO<sub>2</sub> [66]. Thus, annealing is used to achieve crystallinity of the SnO<sub>2</sub> thin films. When the samples are annealed at an appropriate temperature to achieve crystallization, small nanoparticles can be obtained, and the surface appeared as polycrystalline. The particle size increased with increased annealing temperature. These results are attributed to the increased annealing temperature, which enhances crystallinity and defect reduction for thin films [58, 66]. At low annealing temperatures, the strong chemical bonds (covalent or ionic) dominate between primary particles. While at high annealing temperatures, weak bonds exist between primary particles, in which the particles are held together by the weak van der Waals forces to produce agglomerations [67-69]. These agglomerations are undesirable because they contribute to performance reduction for any device [70, 71].

Ansari et al. [72] and Sharma and Madau [73] mentioned that the sensing capability depended on both the ratio of the particle size and depletion width ( $L$ ) of the material. When the crystallite size ( $D$ ) is markedly larger than thickness of the depletion region ( $D \gg 2L$ ), conduction electrons should move from grain to grain (conduction through the hopping of the electrons from grain to grain), across the potential barrier at each grain boundary (grain boundary control), and the height of the boundary varies according to the surrounding atmosphere. In this case, the sensitivity will be independent on the grain size. In addition, when  $D$  decreases to a closer degree to  $2L$ , the conduction electrons move through a channel penetrating each neck (neck control), which is normally formed by connecting the pores between the two neighboring grains. In this case, sensitivity is related to grain size through the neck size. When  $D$  is smaller than  $2L$ , the resistance of grains dominates, and the

gas sensitivity is controlled by grains themselves (grain control) and produces the largest gas sensor response. The other possible explanation for the increase in sensitivity with the decrease in particle size is the surface-to-volume ratio. Smaller diameter means higher surface-to-volume ratio and consequently, higher gas adsorption [74].

Jiang et al. [75] and Serventi et al. [76] showed that the porosity on the surface of SnO<sub>2</sub> samples could be extremely useful for sensing properties. Higher porosity increases surface to volume ratio of the materials. This enhances the gas diffusion inside the SnO<sub>2</sub> sample and thus improves sensitivity. Leem and Yu [77] and Li et al. [78] investigated the effect of annealing temperature on the properties of SnO<sub>2</sub> samples. They found that the increase in annealing temperature of the SnO<sub>2</sub> sample leads to improved crystallinity and increased porosity surface of SnO<sub>2</sub> sample, which enhance the sensing properties of the gas sensor.

### **2.3.6 Gas sensor based on SnO<sub>2</sub> nanostructures**

Fields et al. [79] used thermal evaporation method to fabricate gas sensors based on SnO<sub>2</sub> nanobelts that were grown on SiO<sub>2</sub>/Si substrates. PLD deposition method was utilized to deposit a thin film (~100 nm) of ruthenium oxide (RuO<sub>2</sub>) onto the mask in order to obtain ohmic contact to the nanobelt. The sensor was tested for 20,000 ppm of H<sub>2</sub> gas at a temperature range 25-80 °C. The sensitivities of the SnO<sub>2</sub> nanobelts sensor was almost constant, as calculated by  $[S = G_{gas} - (G_{air}/G_{air})]$ , where  $G_{gas}$  and  $G_{air}$  were the sensor conductance tested in gas and air, respectively. SnO<sub>2</sub> nanobelts sensor can be operated at RT with sensitivity about 60% and the response and recovery times were about 220 s.

Wang et al. [4] investigated H<sub>2</sub> gas sensing based on SnO<sub>2</sub> nanowires prepared via thermal evaporation method based on SiO<sub>2</sub>/Si substrates with Cadmium – Gold (Cd-Au) combo-shaped interdigitating electrodes. The sensitivity increased with increasing H<sub>2</sub> gas concentrations and operating temperatures. The sensitivity toward exposure to 10 ppm H<sub>2</sub> was nearly 0.2 at an operating temperature of 200 °C and increased to 0.4 at 300 °C. When H<sub>2</sub> concentration reached to 1000 ppm, the sensitivity was nearly 0.7 at an operating temperature of 200 °C, which increased to 3.25 at 300 °C.

Ahn et al. [28] fabricated nanophase SnO<sub>2</sub> powder using inert gas condensation method (IGC). SnO<sub>2</sub> powder was milled and mixed to make a paste that was placed on Al<sub>2</sub>O<sub>3</sub> tube and Palladium (Pd), was used as electrodes. The sensitivity of the H<sub>2</sub> gas sensor was presented at operating temperatures of (100, 150, 200, 250, 300 and 350 °C), at a constant H<sub>2</sub> pressure of 2500 ppm. Sensitivity results at different H<sub>2</sub> concentrations ranged from 100 to 10.000 ppm at a constant operating temperature of 250 °C. The sensitivity increased with increasing H<sub>2</sub> concentrations and operating temperatures. The highest sensitivity was obtained for the film sensor sintered at 600 °C with a sensitivity value of 96% for H<sub>2</sub> concentration of 2500 ppm at 250 °C.  $[S (\%) = ((R_{air} - R_{gas})/R_{gas} \times 100)]$  where  $R_{gas}$  and  $R_{air}$  were the sensor resistances tested in gas and air, respectively.

Similar results were presented by Gong et al. [80], where the NC SnO<sub>2</sub> sensor prepared by sol-gel spin coating method on glass substrates with Platinum (Pt) electrodes showed 39% sensitivity  $[(S (\%) = ((R_{air} - R_{gas})/R_{air} \times 100)]$  upon exposure to 1500 ppm of H<sub>2</sub> at operating temperature 200 °C and then increased to 40% at 250 °C. Lingmin et al. [81] studied the influence of the morphology of one-dimensional

SnO<sub>2</sub> nanocrystals prepared via thermal evaporation method on improving H<sub>2</sub> sensing performance. SnO<sub>2</sub> nanostructure powders were mixed with distilled water to create a paste that was placed on Al<sub>2</sub>O<sub>3</sub> tube and platinum (Pt) was used as electrodes. The high response ( $R_{air} / R_{gas}$ ) of SnO<sub>2</sub> nanowires sensor toward exposure to 500 ppm of H<sub>2</sub> gas was 24.35 at an operating temperature of 260 °C, while SnO<sub>2</sub> nanoclusters and nanorods produced responses of 19.30 and 12.40, respectively.

Doping is an effective method that is commonly used to enhance the sensing performance and stability of gas sensors. However, it is achieved through a long and complicated preparation steps that increases the cost of sensor device [82]. Kim et al. [83] successfully fabricated NC powder of SnO<sub>2</sub>-Ag<sub>2</sub>O-PtO<sub>x</sub> composites through sol-gel method and screen printed on Al<sub>2</sub>O<sub>3</sub> substrates with Pt electrodes. The composites showed that the highest response of H<sub>2</sub> gas was for SnO<sub>2</sub>:Ag<sub>2</sub>O: PtO<sub>x</sub>= 93:5:2 in wt% ratio. At the operation temperature of 125 °C, the sensitivity ( $R_{air} / R_{gas}$ ) at exposure to 500 ppm H<sub>2</sub> gas was 18.40 and the response and recovery times were about 8 and 10 s, respectively.

Kocemba et al. [84] demonstrated the H<sub>2</sub> sensing properties based on Pt-doped SnO<sub>2</sub> sensor with doping ratio 1 wt% of Pt at operating temperatures from 100 to 350 °C, was prepared via sol-gel method. Pt-doped SnO<sub>2</sub> was dispersed onto Al<sub>2</sub>O<sub>3</sub> tube that was used as a substrate with Pt as electrodes. The sensor showed high sensitivity at increased operating temperatures and increased calcined temperatures of the Pt-SnO<sub>2</sub> nanoparticles. The maximum sensitivity ( $R_{air} / R_{gas}$ ) to 100 ppm H<sub>2</sub> gas was approximately 5 at an operating temperature of 350 °C. Lin et al. [85] synthesized pure and the transition metal (TM) doped SnO<sub>2</sub> thin films using the sol-gel spin coating method on glass substrates and Pt used as electrodes. The sensitivity

( $R_{air}/R_{gas}$ ) based on pure SnO<sub>2</sub> toward exposure to 500 ppm of H<sub>2</sub> gas was 3.9 at an operating temperature of 250 °C and a recovery time of 84 s, whereas doping of at 5% tungsten (W) increased the sensitivity to 25.8 at the same operating temperature, while the recovery time was 72 s.

Previous studies have attempted to improve the sensitivity of devices without doping steps. Chen et al. [86] noted the significance of porosity for sensor design in the porous SnO<sub>2</sub> thin films using PLD method. In addition, Cantalini et al. [87] noted that a higher porosity in the SiO<sub>2</sub>-Co<sub>3</sub>O<sub>4</sub> films, which were prepared by sol-gel method, allowed for increasing the adsorption/desorption of gas molecules on the surface of a device.

Serventi et al. [27] investigated the contribution of porosity that appeared along the thickness of NC SnO<sub>2</sub> thin films in increasing the sensitivity toward exposure to carbon monoxide (CO) gas. The NC SnO<sub>2</sub> thin films were prepared by RF-sputtering method at substrate deposition temperature of 250 °C on Al<sub>2</sub>O<sub>3</sub> substrates. The NC SnO<sub>2</sub> thin films showed higher porosity than the films prepared at RT. The high porosity of film permitted the gas diffusion inside the thin film. Thereby, high sensitivity was obtained by using the film that was deposited at the highest temperature of 250 °C. Consequently, the sensitivity increased from 175% to 375% toward exposure to 100 ppm of CO gas. Liu et al.[36] showed that the quenched NC SnO<sub>2</sub> thin film 1800 °C/h appears little response ( $R_{air}/R_{gas}$ ) reach to 4.9 to 13.7 ppm H<sub>2</sub>S gas at 100 °C, while the thin film with the slowest cooling rate 25 °C/h exhibits the highest response reach to 42.3 in the same atmosphere and operating temperature. Table 2.2 summarizes the sensitivity of SnO<sub>2</sub> nanostructures based H<sub>2</sub> gas sensor at various preparation methods and at different operating temperatures.

Table 2.2: Summary of the sensitivity, the response and recovery times for the SnO<sub>2</sub> nanostructure based gas sensor.

Materials	Preparation Methods	Substrates	H <sub>2</sub> Concentrations (ppm)	T <sub>opt.</sub> (°C)	S <sub>gas</sub> (%)	Ref.
SnO <sub>2</sub> nanobelts	Thermal evaporation	SiO <sub>2</sub> /Si	20,000	RT	60	[79]
SnO <sub>2</sub> nanowires	Thermal evaporation	SiO <sub>2</sub> /Si	1000	200	70	[4]
Nanophase SnO <sub>2</sub> powder	IGC	Al <sub>2</sub> O <sub>3</sub> tube	2500	250	96	[28]
NC SnO <sub>2</sub> thin film	Sol-gel spin coating	Glass	1500	200	39	[80]
SnO <sub>2</sub> nanowires	Thermal evaporation	Al <sub>2</sub> O <sub>3</sub> tube	500	260	2435	[81]
NC powder of SnO <sub>2</sub> -Ag <sub>2</sub> O-PtOx	Sol-gel	Al <sub>2</sub> O <sub>3</sub>	500	125	1840	[83]
Pt-doped SnO <sub>2</sub>	Sol-gel	Al <sub>2</sub> O <sub>3</sub> tube	100	350	500	[84]
1-SnO <sub>2</sub> thin films 2-W-doped SnO <sub>2</sub> thin films	Sol-gel spin coating	Glass	500 500	250 250	390 2580	[85]

## 2.4 Theoretical background

### 2.4.1 Structural properties of SnO<sub>2</sub>

Tin (Sn) is a natural occurring element that emerges in group 14 (IV) [88] of the Periodic Table at the boundary between metals and nonmetals. The electronic configuration of the  $_{50}\text{Sn}$  element is  $(1s)^2 (2s)^2 (2p)^6 (3s)^2 (3p)^6 (3d)^{10} (4s)^2 (4p)^6 (4d)^{10} (5s)^2 (5p)^2$  [89], whereas that of the  $_{8}\text{O}$  element is  $(1s)^2 (2s)^2 (2p)^4$  [90]. Various types of organic and inorganic compounds may be formed with Sn. Depending on the name of the compound, divalent and tetravalent oxidation states may be labeled by using the names of stannous and stannic, respectively [91]. Another widely encountered nomenclature system, the stock oxidation-number system refers the divalent and tetravalent tin as Sn (II) and Sn (IV), respectively. Sn is a silver-white metal that is malleable and slightly ductile. At normal pressures, Sn has two allotropic forms that have a crystalline structure. One form has a cubic structure and the color is gray or  $\alpha$ -Sn that exists for few temperatures less than 13.2 °C. The other form has a tetragonal structure and the color of gray Sn is changed to white or  $\beta$ -Sn at 13.2 °C. In compounds, tin can occur in the +2 or +4 oxidation states [92]. Sn (IV) dioxide is commonly called tin dioxide, stannic anhydride, or stannic dioxide has a formula SnO<sub>2</sub>.

Tin dioxide (SnO<sub>2</sub>) is a semiconductor and an anisotropic polar crystal that crystallizes into a tetragonal rutile structure. The unit cell contains six atoms, two for tin and four atoms for oxygen. The position of each tin atom is placed at the central of six oxygen atoms and surrounding at the corners of a regular somewhat deformed octahedron. Three tin atoms position are roughly placed at the edge of corners of an equilateral triangle surrounding every oxygen atom; this formation results in a 6:3 coordination as shown in Figure 2.3 [93].